Article

Tribological Behaviour of Hypereutectic Al-Si Composites: A Multi-Response Optimisation Approach with ANN and Taguchi Grey Method

Slavica Miladinović [1], **Sandra Gajević** [1], **Slobodan Savić** [1], **Ivan Miletić** [1], **Blaža Stojanović** [1] and **Aleksandar Vencl** [2,*]

1   University of Kragujevac, Faculty of Engineering, Sestre Janjić 6, 34000 Kragujevac, Serbia
2   University of Belgrade, Faculty of Mechanical Engineering, Kraljice Marije 16, 11120 Belgrade, Serbia
*   Correspondence: avencl@mas.bg.ac.rs

Abstract: An optimisation model for small datasets was applied to thixocasted/compocasted composites and hybrid composites with hypereutectic Al-18Si base alloys. Composites were produced with the addition of Al_2O_3 (36 μm/25 nm) or SiC (40 μm) particles. Based on the design of experiment, tribological tests were performed on the tribometer with block-on-disc contact geometry for normal loads of 100 and 200 N, a sliding speed of 0.5 m/s, and a sliding distance of 1000 m. For the prediction of the tribological behaviour of composites, artificial neural networks (ANNs) were used. Three inputs were considered for ANN training: type of reinforcement (base alloy, Al_2O_3 and SiC), amount of Al_2O_3 nano-reinforcement (0 and 0.5 wt.%), and load (100 and 200 N). Various ANNs were applied, and the best ANN for wear rate (WR), with an overall regression coefficient of 0.99484, was a network with architecture 3-15-1 and a logsig (logarithmic sigmoid) transfer function. For coefficient of friction (CoF), the best ANN was the one with architecture 3-6-1 and a tansig (hyperbolic tangent sigmoid) transfer function and had an overall regression coefficient of 0.93096. To investigate the potential of ANN for the prediction of two outputs simultaneously, an ANN was trained, and the best results were from network 3-5-2 with a logsig transfer function and overall regression coefficient of 0.99776, but the predicted values for CoF in this case did not show good correlation with experimental results. After the selection of the best ANNs, the Taguchi grey multi-response optimisation of WR and CoF was performed for the same combination of factors as the ANNs. For optimal WR and CoF, the combination of factors was as follows: composite with 3 wt.% Al_2O_3 micro-reinforcement, 0.5 wt.% Al_2O_3 nano-reinforcement, and a load of 100 N. The results show that developed ANN, the Taguchi method, and the Taguchi grey method can, with high reliability, be used for the optimisation of wear rate and coefficient of friction of hypereutectic Al-Si composites. Microstructural investigations of worn surfaces were performed, and the wear mechanism for all tested materials was light abrasion and adhesion. The findings from this research can contribute to the future development of hypereutectic Al-Si composites.

Keywords: hypereutectic Al-Si; composites; friction; wear; optimisation; Taguchi grey; ANN

1. Introduction

The automotive industry and other industries are in constant expansion, and thus there is a constant tendency to reduce exhaust greenhouse gases. The most commonly used lightweight material is aluminium and its alloys due to its characteristics, such as low density (a third of the density of steel), corrosion resistance (aluminium with oxygen forms a very thin film of aluminium oxide, which prevents further oxidation), high electrical and thermal conductivity, paramagnetic properties, and easy machining. In addition, highly reflective surfaces can be achieved, which can be used both decoratively and functionally [1]. Aluminium silicon alloys (Al-Si alloys) are widely used and there are three types of these

alloys depending on the weight percentage (wt.%) of Si. Alloys with Si under 12 wt.% are hypoeutectic alloys, the ones with around 12 wt.% are eutectic alloys, and the ones above 13 wt.% (more precisely 12.6) are hypereutectic Al-Si alloys [2].

Hypereutectic Al-Si composites provide a combination of lightweight properties inherent to aluminium and the favourable mechanical properties of silicon-rich materials. Some hypereutectic Al-Si alloy properties are low thermal expansion coefficient, good weldability, high wear resistance, and high-temperature strength, which are due to primary Si presence in the aluminium base [3,4]. With the application of different reinforcing materials, it is possible to improve the performance characteristics of composites with a hypereutectic Al-Si matrix for various engineering applications. Miladinović et al. [4] have reviewed reinforcements and fabrication methods and their influence on microstructure, and the mechanical and tribological properties of hypereutectic Al-Si alloys and their composites. Among others, semi-solid processes like rheocasting and thixocasting are relatively new. Thixocasting transforms the initial dendritic structure into a rounded, more homogeneous structure, improving the overall properties of the alloy [5]. Thixocasted materials have good mechanical properties, and fewer defects like porosity, macro segregation, and shrinkage, but this process has a high cost because the residual materials are not recyclable. A lot of researchers are working on overcoming these problems [6]. Birol [7] investigated the A390 alloy (17 wt.% Si) produced by thixocasting. Thixocasted samples had a uniform distribution of Si particles and no porosity. Hardness was higher for thixocasted samples compared to die-casted ones, and T5 and T6 heat treatments further improved hardness. The influence of heat treatment on hypereutectic alloys produced by conventional casting was investigated in [8–11], while other researchers compared different production processes for hypereutectic Al-Si alloys [12–15]. Investigating the tribological characteristics of samples with and without T6 heat treatment, it was concluded that the wear of T6 samples increases by approximately 14% compared to the hypereutectic Al-Si alloy without heat treatment. Nano-size ceramics of Al_2O_3 are successfully used for aluminium composites due to their proven influence on wear resistance and high-temperature properties without the formation of intermetallic phases [16–19]. Stojanović et al. [20] used small amounts of reinforcement particles of 0.2, 0.3, and 0.5 wt.% Al_2O_3 in the A356 aluminium alloy matrix to develop a nanocomposite with appropriate wear resistance. By employing a low percentage of reinforcement amounts, they also examined the influence of Al_2O_3 particle sizes, specifically 30 and 100 nm. They concluded that when the reinforcement content is below 0.5 wt.% Al_2O_3, there is no improvement in the tribological characteristics. It was also observed that with the application of reinforcement particles of nano/micro Al_2O_3 and SiC, the wear rate increases [21–23].

An ANN prediction of mechanical and tribological properties of aluminium alloy (AA 1100) reinforced with 6 wt.% particles of rice husk ash (RHA), bagasse ash (BA), coconut shell ash (CSA), ZnO, and eggshell, and fabricated by the liquid metallurgy technique was conducted by Nagaraj and Gopalakrishnan [24]. The output parameters were wear and coefficient of friction. Experiments were conducted at different normal loads, sliding speeds, and sliding times. It was concluded that ANN can be successfully used for the prediction with 94% accuracy. A lot of researchers combine ANNs with other optimisation methods, like Taguchi, Taguchi grey, PSO (particle swarm optimisation), RSM (response surface methodology), and others. Karabulut and Karakoç [25] applied Taguchi method and ANN for the optimisation of the machining parameters of Al7075 and open-cell SiC composite. The observed output parameter was surface roughness. After training the ANN and conducting a regression analysis, a good correlation between predicted and experimental values was achieved. The application of the Taguchi and ANN methods was successful in the research conducted by Ekka et al. [26]. They used nano-reinforcements of SiC and Al_2O_3 (0.5, 1 and 1.5 wt.%) in an aluminium-based composite. It was found that composites with 0.5 wt.% SiC or Al_2O_3 resulted in minimal wear. Additionally, they determined that the developed ANN model and regression model can be used for predicting the wear rate with high reliability. Ajith Arul Daniel et al. [27] applied ANNs and the Taguchi grey method for

the multi-response prediction and optimisation of control factors in the milling of Al5059 with SiC (5, 10 and 15 wt.%) and MoS_2 (2 wt.%) hybrid metal matrix composites. The study concludes that the developed ANN model showed better performance than the regression model. With grey relational analysis, the optimal combination of influential factors was obtained [27]. Hussain et al. [28] employed Taguchi grey relational analysis to optimise the powder metallurgy factors affecting mass density and hardness in Cu-based composites with Al_2O_3 particles. With confirmation tests, the effectiveness of grey-based Taguchi optimisation was proven, emphasising the simplified process optimisation it offers through Monte Carlo simulated models and orthogonal array designs. Dey et al. [29] employed Taguchi grey relational analysis to evaluate the tribological behaviour of Al2024 alloy with TiB_2 composites. Based on the grey-Taguchi approach, the optimal factor combination was determined and confirmed through confirmation experiments, demonstrating the efficiency of the grey-Taguchi method in optimising the tribological behaviour of composites.

This paper applies the design of experiment (DOE) technique for tribological tests and the optimisation of influential factors on the wear and friction of hypereutectic Al-Si composites. An ANN was developed for the prediction of the wear rate and coefficient of friction with the application of the Levenberg–Marquardt backpropagation algorithm for its training. The ANN's predicted values were compared with experimental results and Taguchi prediction. Percentage influence was determined with the use of the ANOVA method. Multi-response optimisation was applied via the Taguchi grey method to obtain the best combination of factors for both wear rate and coefficient of friction. This paper aims to develop ANN and Taguchi models for small data sets and to observe which one of these methods is more suitable for the prediction of tribological behaviour of hypereutectic Al-Si composites.

2. Materials and Methods

The majority of investigations, based on a literature review [4], were conducted for hypereutectic Al-Si alloys (fabrication methods, heat treatment, and the addition of alloying elements). Only recently have there been more intensive investigations regarding composites with a hypereutectic Al-Si alloy matrix. The most commonly used reinforcement materials for pistons are Al_2O_3 and SiC [30]. The application of micro-reinforcements of SiC and Al_2O_3 in an aluminium matrix influenced the improvement of the wear resistance. With an increase in the amount of SiC and Al_2O_3 in aluminium composites, wear resistance, hardness, and tensile strength increase; additionally, density and porosity also increase [22,23,31–33]. The 3 wt.% of SiC and 3 wt.% Al_2O_3 were selected to enhance the specific properties (such as hardness and wear resistance) and maintain the overall integrity and workability of the composite material, which allows the optimisation of multiple properties without significantly compromising the others. An improvement in wear resistance has been recorded with the addition of 0.5 wt.% Al_2O_3 nano-reinforcements, as well as 0.5 wt.% SiC nano-reinforcements in the A356 alloy [20,34] and hypereutectic Al-Si alloy. Consequently, 0.5 wt.% Al_2O_3 nano-reinforcement was selected for the formation of hybrid composites. The materials for this study were fabricated at the Institute of Nuclear Sciences "Vinca" by semisolid route of the thixocasting/compocasting process. Composite materials were obtained with the combination of matrix alloy Al-18Si and 3 wt.% Al_2O_3 or SiC micro-reinforcement. Hybrid composites were obtained with the matrix alloy Al-18Si, 0.5 wt.% Al_2O_3 nano-reinforcement, and the addition of 3 wt.% Al_2O_3 or SiC micro-size particles. The average size of Al_2O_3 nanoparticles was 25 nm, while the sizes of Al_2O_3 and SiC microparticles were approximately 36 and 40 μm, respectively. The microstructures of the produced materials are presented in Figure 1.
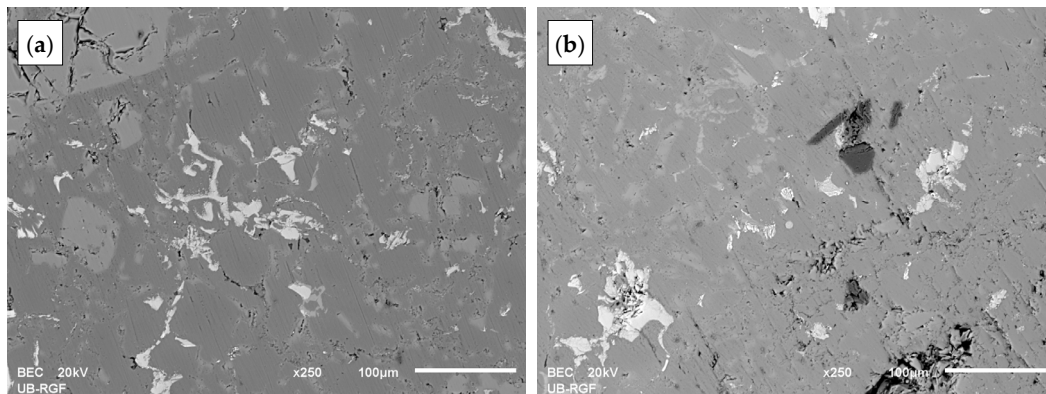
Figure 1. Microstructures of produced composites: (**a**) matrix material Al-18Si and (**b**) composite with 0.5 wt.% Al_2O_3 (25 nm) and 3 wt.% Al_2O_3 (36 μm).

In the matrix alloy, bigger primary Si particles, eutectic Si particles, and intermetallic phases are present (Figure 1a). Matrix alloys with primary Si particles of a larger size can be noticed in microstructural images of hypereutectic Al-Si alloys [35–38]. The primary Si particles in composite with 0.5 wt.% Al_2O_3 (25 nm) and 3 wt.% Al_2O_3 (36 μm), shown in Figure 1b, were refined, but the Al_2O_3 agglomerates can be noticed. Refinement of primary Si with the addition of Al_2O_3 [37,38] or the addition of Al_2O_3/TiO_2 nanoparticles in hypereutectic Al-Si alloy was observed in the research conducted by Mahallawi et al. [39]. An agglomeration of Al_2O_3 nanoparticles was also reported in [37,40]. The needle-like intermetallic phases present in the microstructures of both matrix alloy and composite are β-Al_5FeSi which are also noticed in the literature [36,41–43]. Irregularly shaped light-coloured phases contain Al-Ni-Cu-(Fe). According to [44], the Al-Ni-Cu-Fe phase is the δ-AlCuNi ($Al_3(CuNi)_2$) phase, while the irregularly shaped Al-Ni-Cu phase is the γ-AlCuNi phase (Al_7Cu_4Ni), which is presented as the brightest phase with very small dimensions.

The experimental procedure consisted of tribological tests and microscopical observations of worn surfaces. Composites were machined to appropriate dimensions. Specimens were tested on a block-on-disc tribometer according to the ASTM G77 standard. A schematic of the contact pair (nominal line contact) is given in Figure 2. The counter-body was disc made of quenched and tempered steel EN 42CrMo4 with a diameter of 55 mm and hardness of 51–54 HRC. The contact surfaces of the block and disc for the tribological test had a roughness of approximately Ra = 0.4 μm. Tribological tests were performed in lubricated conditions with motor oil, SAE 5W-30, with a viscosity of 68 mm^2/s at 40 °C and 11.5 mm^2/s at 100 °C, and a density of 0.848 g/cm^3 at 15 °C. The pistons in the engines work on approximately 8 MPa pressure [45,46], so a normal load of 100 N which corresponds to that pressure was selected, as well as 200 N, since some pistons work at higher pressures. The duration of tests was 2000 s, i.e., the sliding distance was 1000 m. The tests were performed in ambient air at room temperature, and oil temperature did not exceed 40 °C. The disc was immersed in an oil container, and, with its rotation, the oil was brought into contact between the disc and the block.

After the tests, block wear was monitored by wear scar width (Ww). By knowing the contact geometry and wear scar width, the wear rate (expressed in mm^3/m) could be calculated. During the tests, the coefficient of friction was automatically acquired by the software used. To obtain more reliable insight into the wear behaviour of the materials, five repetitions were completed for each testing condition. After the tribological tests, worn surfaces were observed with a scanning electron microscope (SEM) Jeol JSM-6610LV equipped with an energy dispersive spectrometer (EDS) Xplore30.
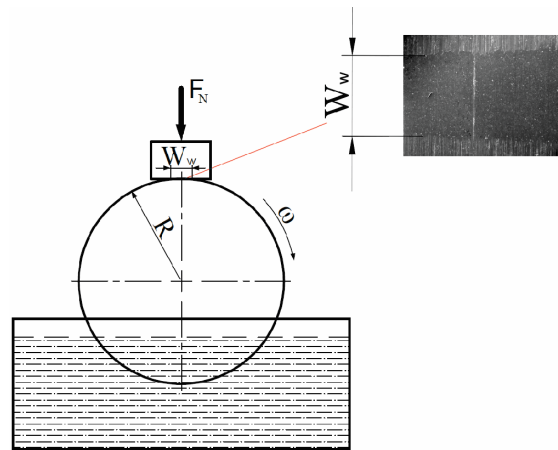
Figure 2. Schematics of contact pair.

3. Design of Experiment and Optimisation

3.1. Artificial Neural Networks

The use of artificial neural networks (ANNs) for the prediction of material behaviour is constantly expanding. ANNs are frequently employed to model complex nonlinear relationships and problems with wide, experimental datasets, but some investigations have proven that it can be used, with high reliability, for small data sets. They can be used for pattern recognition, data classification, and prediction, providing valuable insights across different fields. These networks, which represent simplified models of human brain function (Figure 3), are trained rather than programmed, enabling them to learn and adapt to complex data patterns effectively. Training the network involves enabling it to understand the relationships between inputs and outputs. This training process focuses on adjusting the weights of connections or synapses between neurons. In the input layer, each neuron receives a signal, which is then transmitted to the hidden layer by multiplying it with the corresponding synaptic weights. The hidden neurons calculate their output signals by summing these weighted inputs and applying a transfer function. The output signals from the hidden neurons are then forwarded to the neurons in the output layer. Each output neuron processes its weighted input signals, applying its transfer function to compute its specific output signal as follows [47–50]:

$$Y_j = f(\sum_{i=0}^{n} W_{ij}X_i) + B, \tag{1}$$

where B is bias, X_i is output neuron, Y_j is hidden neuron, and W_{ij} is the synapse weight between these two neurons.
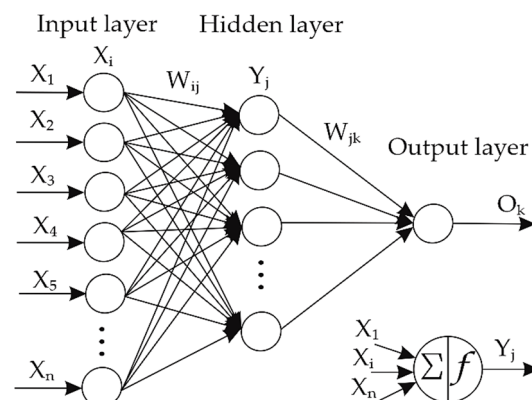

Figure 3. Schematic model of simplified ANN.

The signal generated by the hidden neuron Y_j is distributed to all neurons within the output layer. Each of these output neurons (O_k) calculates its output signal by aggregating its weighted input signals and then applying the appropriate transfer function for computation [47].

$$O_k = f(\sum_{j=1}^{n} W_{ik} Y_j) + B, \qquad (2)$$

where B is bias, O_k is output neuron, Y_j is hidden neuron, and W_{ik} is the synapse weight between these two neurons.

Mostly used ANNs are the simplest ones, which consist of an input layer, hidden layer, and an output layer, each layer having its own number of neurons. Commonly used transfer functions are pure linear (purelin), hyperbolic tangent sigmoid (tansig), and logarithmic sigmoid (logsig). The most applied training algorithm is backpropagation, which employs a gradient descent technique to minimise error for specific training patterns. It involves adjusting the initially assigned weights of synapses iteratively until a low sum of square error (R) is achieved. The mean square error (MSE) across all patterns is calculated to evaluate the network's performance as follows [51]:

$$R^2 = 1 - \frac{\sum_i (p_i - a_i)^2}{\sum_i (a_i)^2}, \qquad (3)$$

where p_i and a_i are predicted and actual output value, respectively.

In this study the ANN network had 3 input neurons (micro-reinforcement type, amount of Al_2O_3 nanoparticles and normal load), varied neurons in the hidden layer (from 5 to 20), and 2 output neurons (wear rate and coefficient of friction). For this study, a few feed-forward backpropagation ANNs were applied with logsig and tansig transfer functions.

3.2. Taguchi Design

The Taguchi method optimises product quality through statistical parameter design while minimising the number of experiments in engineering industries. Within engineering industries, the paramount goal is to consistently produce high-quality products, commencing with the inception of preliminary concepts and advancing through the stages of design and engineering [52]. The Taguchi experimental design is a statistical technique used to investigate how variations in input factors affect the resulting output responses. Its goal is to pinpoint the best process settings that minimise variability in these outputs. This approach allows for the examination of chosen factors with a minimal number of experimental runs using an orthogonal array [34]. Generally, the Taguchi methodology follows a set of critical stages. These stages encompass identifying the factors and their corresponding levels, conducting experiments using an orthogonal array (OA) table as a guide, evaluating the signal-to-noise (S/N) ratio, determining the response table, and applying ANOVA. ANOVA helps to validate the significance of factors in terms of their contribution. The final phase encompasses a confirmation test, which is conducted based on the estimated process parameter values [52–54].

In the Taguchi method, the signal-to-noise (S/N) ratio is used to measure quality characteristics deviating from the desired values. The S/N ratio is interpreted as the ratio of the mean value of the signal to the standard deviation of the noise value. It is used to arbitrate the rank of input process factors. Three types of quality characteristics are used in the analysis of the S/N ratio: smaller-is-better, larger-is-better, and nominal-is-best [52,54]. Depending on the output goal, the appropriate quality characteristic is selected. In this study, we have chosen a "smaller-is-better" type of characteristic, and the S/N ratio is computed using the following equation:

$$S/N = -10 \log(\frac{1}{n} \sum_{i=1}^{n} y_i^2), \qquad (4)$$

where y_i is the *i*-th observed output value (experimental results) and *n* is the number of experiments.

3.3. Grey Relational Analysis

Grey relational analysis is a multi-response optimisation approach used to evaluate near-optimal relationships between responses [28]. In this investigation of wear rate and coefficient of friction, the lower values for both tribological properties are preferred, which requires that their normalisation is performed for the-lower-the-better quality characteristic, as follows [55]:

$$Y_i^*(k) = \frac{\max Y_i(k) - Y_i(k)}{\max Y_i(k) - \min Y_i(k)},$$ (5)

where, in case of multiple responses, *k* is number of the response, max $Y_i(k)$ and min $Y_i(k)$ are maximum and minimum value of experiment response, and $Y_i(k)$ is the reference value.

After the normalization of data, the grey relation coefficient of an individual response $\xi_i(k)$ can be calculated as follows:

$$\xi_i(k) = \frac{\Delta_{\min} - \varsigma \Delta_{\max}}{\Delta_{0i}(k) - \varsigma \Delta_{\max}},$$ (6)

where $\Delta_{0i}(k)$ is the deviation of the reference value (Equation (6)), ς is the distinguishing coefficient which is in the range of $0 \leq \varsigma \leq 1$ (this coefficient is usually equal to 0.5), and $\Delta_{\min}$ and $\Delta_{\max}$ are minimum and maximum values of deviation.

$$\Delta_{0i}(k) = |Y_0^*(k) - Y_i^*(k)|,$$ (7)

where $Y_0^*(k)$ is the reference value, and $Y_i^*(k)$ is a comparability value.

The grey relation grade (GRG), which gives the relationship between two responses, can be calculated with the following equation:

$$\gamma_i = \frac{1}{k}\sum_{i=1}^{n} \xi_i(k),$$ (8)

where *k* is number of the responses and *n* is number of experiments.

When each response has its own weight (W_k), then GRG can be calculated as follows:

$$\gamma_i = \frac{1}{k}\sum_{i=1}^{n} W_k \xi_i(k).$$ (9)

At the end of the analysis, the values are ranked from highest to lowest to obtain the best combination of input factors vs. responses.

4. Results and Discussion

The design of experiments (DOE) technique is useful for any experimental analysis in all areas of research. It is a very powerful technique for achieving significant improvements in product quality, i.e., in this case, composite materials and process efficiency, more precisely, tribological conditions. Three factors were selected for the experimental design, which are given in Table 1, along with their levels and labels. The three-level factor is the type of micro-reinforcement, while the other two-level factors are the amount of Al_2O_3 nanoparticles and normal load.

Experimental results for wear rate and coefficient of friction were obtained by conducting experiments using the Taguchi orthogonal matrix L12, and they are shown in Table 2. To facilitate the presentation of model coefficients and easier interpretation of the results, the factor levels are coded (1), (2), and (3), and shown in Table 1.

Table 1. Input factors and their labels and levels.

Factor and Label	Unit	Level I	Level II	Level III
Type of micro-reinforcement (A)	–	matrix only (1)	3 wt.% Al_2O_3 (2)	3 wt.% SiC (3)
Amount of Al_2O_3 nanoparticles (B)	wt.%	0 (1)	0.5 (2)	–
Normal load (C)	N	100 (1)	200 (2)	–

Table 2. Experimental, ANN, and S/N ratio results.

Exp. no	Imput Factor			Experiment				ANN Combined 3-5-2 Logsig				ANN 3-15-1 Logsig			ANN 3-6-1 Tansig	
	A	B	C	$WR \times 10^{-5}$ [mm³/m]	CoF	$WR \times 10^{-5}$ [mm³/m]	CoF	Error WR	Error CoF			$WR \times 10^{-5}$ [mm³/m]	Error	CoF	Error	
1	1	0	100	4.3969	0.101	4.3969	0.101	0.0000	0.0000			4.3899	0.0070	0.1031	−0.0021	
2	1	0	200	6.2826	0.1109	6.2826	0.1109	0.0000	0.0000			5.8444	0.4382	0.1123	−0.0014	
3	1	0.5	100	4.7872	0.0927	4.7872	0.0927	0.0000	0.0000			4.7882	−0.0010	0.0922	0.0005	
4	1	0.5	200	7.2794	0.1021	6.2973	0.0999	0.9821	0.0021			7.1276	0.1518	0.1010	0.0011	
5	2	0	100	3.9305	0.1071	3.9305	0.1071	0.0000	0.0000			3.9282	0.0023	0.1036	0.0035	
6	2	0	200	7.3077	0.1243	7.3077	0.1243	0.0000	0.0000			7.2973	0.0104	0.1163	0.0080	
7	2	0.5	100	3.9063	0.1063	3.7091	0.0983	0.1972	0.0080			3.9081	−0.0018	0.1048	0.0015	
8	2	0.5	200	7.6366	0.1122	7.6366	0.1122	0.0000	0.0000			7.9297	−0.2931	0.1135	−0.0013	
9	3	0	100	4.3165	0.1023	4.5994	0.1089	−0.2829	−0.0067			4.3140	0.0025	0.1040	−0.0017	
10	3	0	200	7.3432	0.117	7.3432	0.117	0.0000	0.0000			7.3180	0.0252	0.1177	−0.0007	
11	3	0.5	100	4.7056	0.1077	4.7056	0.1077	0.0000	0.0000			4.5901	0.1155	0.1119	−0.0042	
12	3	0.5	200	7.8468	0.1176	7.6817	0.1172	0.1651	0.0004			7.8461	0.0007	0.1180	−0.0004	

Exp. no	Taguchi		Grey								
	S/N for WR	S/N for CoF	norm. WR	norm. COF	delta WR	delta COF	GRC WR	GRC CoF	GRG	Rank	
1	−12.8629	19.9136	0.8755	0.7373	0.1245	0.2627	0.8006	0.6556	0.7622	5	
2	−15.9628	19.1014	0.3970	0.4241	0.6030	0.5759	0.4533	0.4647	0.4563	7	
3	−13.6016	20.6584	0.7764	1.0000	0.2236	0.0000	0.6910	1.0000	0.7730	4	
4	−17.2419	19.8195	0.1440	0.7025	0.8560	0.2975	0.3687	0.6270	0.4372	8	
5	−11.8890	19.4042	0.9939	0.5443	0.0061	0.4557	0.9879	0.5232	0.8646	2	
6	−17.2756	18.1106	0.1368	0.0000	0.8632	1.0000	0.3668	0.3333	0.3579	11	
7	−11.8353	19.4693	1.0000	0.5696	0.0000	0.4304	1.0000	0.5374	0.8773	1	
8	−17.6580	19.0001	0.0533	0.3829	0.9467	0.6171	0.3456	0.4476	0.3727	9	
9	−12.7026	19.8025	0.8959	0.6962	0.1041	0.3038	0.8277	0.6220	0.7731	3	
10	−17.3177	18.6363	0.1278	0.2310	0.8722	0.7690	0.3644	0.3940	0.3722	10	
11	−13.4523	19.3557	0.7972	0.5253	0.2028	0.4747	0.7114	0.5130	0.6588	6	
12	−17.8939	18.5919	0.0000	0.2120	1.0000	0.7880	0.3333	0.3882	0.3479	12	

4.1. Artificial Neural Network Analysis

During tribological testing, wear rate (WR) and coefficient of friction (CoF) were obtained, and their results are given in Table 2. These results were used for the ANN. As already stated, ANNs are trained, not programmed, which is the reason why more ANNs were used to observe which network gives the most satisfactory results. The optimal number of neurons in the hidden layer and transfer function are often determined through a trial-and-error process which balances model complexity and performance, which has also been achieved by this research. Many different networks were trained for both transfer functions to obtain the best overall regression coefficient. Different numbers of hidden neurons and transfer functions were applied, and Table 3 shows the results of the ANNs in the form of their overall regression coefficient. MSE was calculated according to Equation (3) and is also shown in Table 3. Firstly, all networks were trained for 5, 10, 15, and 20 neurons in a hidden layer, and the ANN with the highest overall regression coefficient was selected. If the overall regression coefficient of that network was too low then, one by one, another neuron was added to achieve a higher regression coefficient. The best performance for WR was for the ANN with the architecture of 3-15-1 with logsig transfer function (3 inputs, 15 neurons in hidden layer, and 1 output), where the overall regression coefficient was 0.99484, and the regression coefficients for training, validation, and testing were 0.99999, 1, and 1, respectively (Figure 4a). The obtained regression coefficients indicate an excellent fit of the model to the data for WR. Such high values, particularly the overall regression coefficient being close to 1, suggest that the ANN has learned to predict the target variable

with a high degree of accuracy. Training, validation, and testing phases imply that the ANN's predictions are almost exactly in line with the actual data of the dataset, which is also confirmed by the high MSE (Table 3). For CoF, the ANN with an architecture of 3-6-1 and tansig transfer function gave the best output and overall regression coefficient of 0.93096. The CoF regression coefficients for validation and testing were both equal to one which indicates that network behaviour for these phases is almost exactly as it was for the experimental data; however, the regression coefficient for training was 0.89358, which indicates that there will be some degree of deviation between experimental and predicted values (Figure 4b). In order to investigate the ANN's potential for multiple response prediction, the network with two outputs was trained with an architecture of 3-5-2 and logsig transfer function. After training, the overall regression coefficient was obtained, and it was 0.99776, while the training, testing, and validation regression coefficients were 0.99948, 0.99465, and 1, respectively (Figure 4c). This ANN was selected due to it having the highest MSE for CoF, which indicated a good fit with experimental results (Table 3).
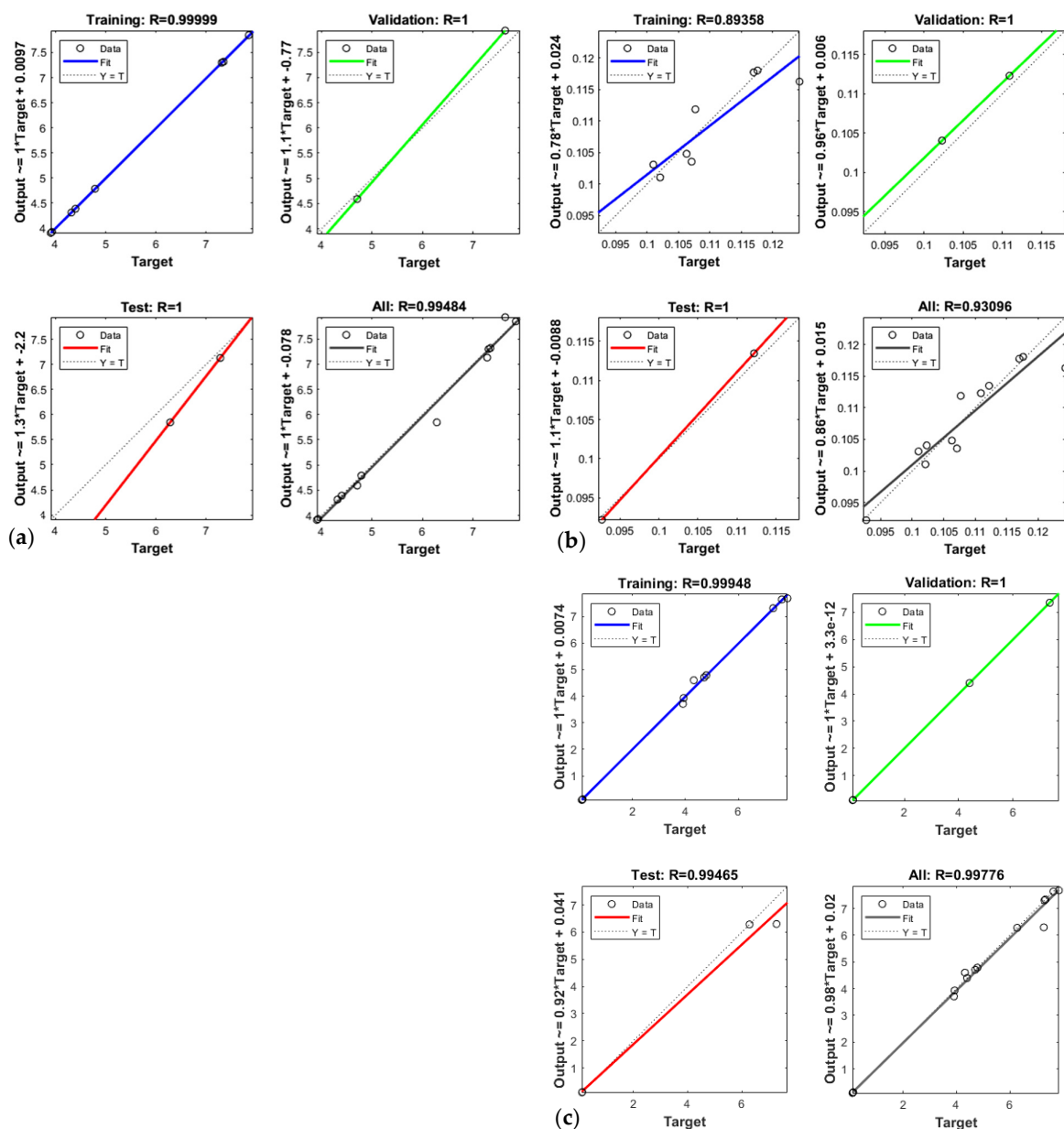
Figure 4. Regression coefficients for the best ANN for (**a**) wear rate (WR), (**b**) coefficient of friction (CoF), and (**c**) both outputs.

Table 3. Results of training for different ANNs.

Prediction	WR									
Transfer function	tansig				logsig					
No. of neurons in the hidden layer	5	10	15	20	5	10	15	16	17	20
Regression coefficient MSE	0.97358 0.96924	0.9895 0.99062	0.98869 0.98987	0.98547 0.98697	0.9316 0.96924	0.97731 0.97043	0.99484 0.99927	0.97145 0.97543	0.99189 0.99286	0.98717 0.98494
Prediction	**CoF**									
Transfer function	tansig					logsig				
No. of neurons in the hidden layer	5	6	7	10	15	5	6	7	10	15
Regression coefficient MSE	0.91038 0.99988	0.93096 0.99992	0.92719 0.99990	0.88538 0.99986	0.76831 0.99986	0.88754 0.99986	0.91765 0.99990	0.86306 0.99984	0.75498 0.99971	0.80757 0.99971
Prediction	**WR and CoF combined**									
Transfer function	tansig			logsig						
No. of neurons in the hidden layer	5	10	15	5	10	15				
Regression coefficient MSE for WR MSE for CoF	0.99799 0.98714 0.99822	0.99022 0.93494 0.99916	0.98325 0.88919 0.99761	0.99776 0.98383 0.99991	0.99167 0.93723 0.99903	0.99761 0.99488 0.99864				

Predicted values of WR and CoF are better for individually trained ANNs than for combined ones (Table 2). The trained ANNs indicate a good correlation between experimental and predicted values based on Figure 4 and Table 2. Figure 4a shows that there is a good correlation between the experimental and predicted values of wear rate, while in Figure 4b, the coefficient of friction has a slight difference between the experimental and predicted values; however, there is still a good correlation between these results. Results show that ANNs can be used for smaller data sets, which corresponds to other authors' findings [20,25,56].

4.2. Taguchi Grey Analysis

The analysis of the experimental results is based on the assessment of the influence of the factors, as well as the ANOVA of the obtained results in the MINITAB 20.4 software package. The S/N ratio for achieving minimum WR and minimum CoF is expressed by the characteristic "smaller-is-better", and it is calculated using Equation (4). Regardless of the applied quality characteristic, the transformed results are always interpreted so that a higher value of the S/N ratio is better. The ranking of the influential factors of WR and CoF was performed by evaluating the input values based on Table 4.

Table 4. Response table of signal-to-noise ratios for WR and CoF (smaller-is-better).

	WR				**CoF**		
Level	**A**	**B**	**C**	**Level**	**A**	**B**	**C**
1	−14.92	−14.67	−12.72	1	19.87	19.16	19.77
2	−14.66	−15.28	−17.22	2	19.00	19.48	18.88
3	−15.34			3	19.10		
Delta	0.68	0.61	4.50	Delta	0.88	0.32	0.89
Rank	2	3	1	Rank	2	3	1

Based on the delta value, the ranks of the considered factors have been determined. The factor with the highest delta value is the load that mostly affects the WR and CoF. The second- and third-ranked factors are the type of micro-reinforcement and the amount of Al_2O_3 nanoparticles, respectively. Determining the optimal combination of factor levels individually for each output is possible using the graphs shown in Figure 5.
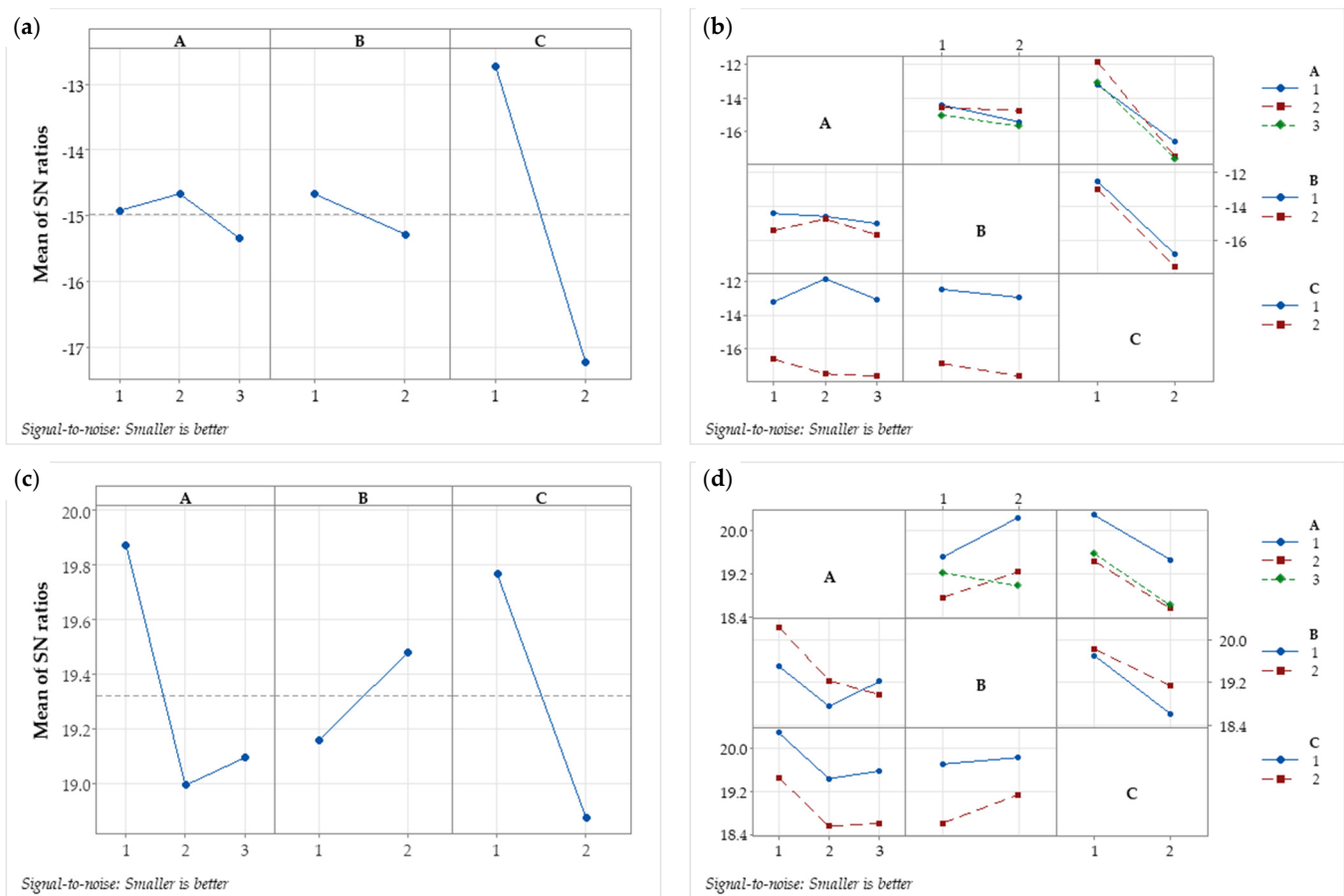
Figure 5. Diagrams of S/N ratio: (**a**) main effect for wear rate, (**b**) interaction plot for wear rate, (**c**) main effect for CoF, and (**d**) interaction plot for CoF.

Figure 5 shows three graphs representing the mean response and mean S/N ratio for micro-reinforcement type, Al_2O_3 nanoparticles amount, and normal load (A, B, and C). Values displayed graphically are based on the S/N ratio. The optimal combination of factor levels for WR (Figure 5a) is A2-B1-C1, which means that the minimal wear rate of the composites is achieved with the 3 wt.% Al_2O_3 micro-reinforcement with 0 wt.% of Al_2O_3 nanoparticles at a normal load of 100 N. The optimal combination of factor levels for the friction coefficient (Figure 5c) is A1-B2-C1, which means that the minimum coefficient of friction of the composite is achieved without additional reinforcement, i.e., matrix alloy, with 0.5 wt.% Al_2O_3 nanoparticles at a normal load of 100 N. Looking at the interaction graph for WR and CoF (Figure 5b,d), it can be observed that there is an interaction between certain factors, since the lines of those factors are not parallel. Based on the deviation in the parallelism of the interaction lines, it can be determined whether the factor interactions affect WR and CoF. The higher the deviation from line parallelism, the higher the impact of the interaction. It can be inferred that only the A × C interaction (type of micro-reinforcement and normal load) has an impact on WR, while the influence of other interactions is negligible. The influence of the A × B (type of micro-reinforcement and amount of Al_2O_3 nanoparticles) interaction on CoF is the highest (Figure 5d), followed by B × C (amount of Al_2O_3 nanoparticles and normal load), while the influence of A × C is negligible.

ANOVA provides a more precise influence of interactions and the effect of the factors on each observed output individually. ANOVA was used to determine the significance of various factors on the wear rate and coefficient of friction. This analysis was performed at a 95% confidence level, corresponding to a significance level of 5%, and the results were the

sum of squares, F-values, and *p*-values, confirming the significance of each control factor's influence on the output response (Tables 5 and 6).

Table 5. ANOVA for wear rate (WR).

Source	DF	Seq SS	Adj SS	Adj MS	F-Value	*p*-Value	Percentage Contribution
A	2	0.9367	0.9367	0.4683	12.60	0.074	1.42
B	1	1.1239	1.1239	1.1239	30.23	0.032	1.71
C	1	60.7775	60.7775	60.7775	1634.96	0.001	92.33
A × B	2	0.3605	0.3605	0.1803	4.85	0.171	0.55
A × C	2	2.4978	2.4978	1.2489	33.60	0.029	3.79
B × C	1	0.0537	0.0537	0.0537	1.45	0.352	0.08
Residual error	2	0.0743	0.0743	0.0372			0.11
Total	11	65.8244					100.00

R-Sq (99.89%) R-Sq(adj) 99.38%

DF—degree of freedom; Seq SS—sequential sums of square; Adj SS—adjusted sums of square; and Adj MS—adjusted mean square.

Table 6. ANOVA for coefficient of friction (CoF).

Source	DF	Seq SS	Adj SS	Adj MS	F-Value	*p*-Value	Percentage Contribution
A	2	1.84351	1.84351	0.92176	20.36	0.047	35.00
B	1	0.30925	0.30925	0.30925	6.83	0.121	5.87
C	1	2.37985	2.37985	2.37985	52.56	0.019	45.18
A × B	2	0.51399	0.51399	0.25699	5.68	0.150	9.76
A × C	2	0.00985	0.00985	0.00493	0.11	0.902	0.19
B × C	1	0.12002	0.12002	0.12002	2.65	0.245	2.28
Residual error	2	0.09056	0.09056	0.04528			1.72
Total	11	5.26703					100.00

R-Sq (98.28%) R-Sq(adj) 90.54%

DF—degree of freedom; Seq SS—sequential sums of square; Adj SS—adjusted sums of square; and Adj MS—adjusted mean square.

Based on the ANOVA and Table 5, it was inferred that factor C (normal load), had a significant influence on the WR, with a substantial influence of 92.33%. The high percentual influence of normal load on wear rate is possibly due to the higher applied loads compared to other studies [11,15,57–60]; however, it corresponds to the findings presented in [26,34,53]. The rest of the influence is distributed among other factors as follows: the amount of Al_2O_3 nanoparticle influence was 1.71%, the micro-reinforcement type influence was 1.42%, and the influence of the interactions between the factors A and C was 3.79%. The influence of the interaction of B and C and A and B is negligible. The ANOVA revealed that, in the analysis of the CoF, besides the load, the micro-reinforcement type also stands out with a considerable influence of 45.18 and 35.00%, respectively (Table 6). This is in accordance with the literature [61]. The influence of the amount of Al_2O_3 nanoparticles on CoF was 5.87%. When considering the influence of factor interactions in the analysis of CoF, the A and B combination of factors stands out with an influence of 9.76%, while the B and C combination influence was 2.28%. The influence of the A and C interaction on CoF is negligible. Multiple linear regression was used to predict the wear rate and coefficient of friction based on the control factors (A, B, and C), taking into account the interactions between these factors. The regression equation for wear rate and coefficient of friction was obtained after the analysis, and are as follows:

$$WR = 2.16 - 0.303 \cdot A + 0.141 \cdot B + 1.510 \cdot C - 0.124 \cdot A \cdot B + 0.447 \cdot A \cdot C + 0.358 \cdot B \cdot C \quad (10)$$

and

$$CoF = 0.0971 - 0.00591{\cdot}A + 0.0073{\cdot}B + 0.0168{\cdot}C + 0.00578{\cdot}A{\cdot}B + 0.00132{\cdot}A{\cdot}C - 0.00553{\cdot}B{\cdot}C. \qquad (11)$$

After the development of regression equations (Equations (10) and (11)), the coefficient of determination (R^2) was calculated according to the literature [62], and for WR and CoF, R^2 was 0.98596 and 0.92529, respectively. These R^2 values are close to 1 which indicates that there is a good correlation between the developed model and experimental results. A comparison of predicted values using the ANN and the regression model with experimental values is given in Figure 6. From Figure 6 it can be inferred that the regression and ANN prediction of the individual outputs (WR and CoF) have a better correlation with the experimental results than with the ANN for two outputs simultaneously.
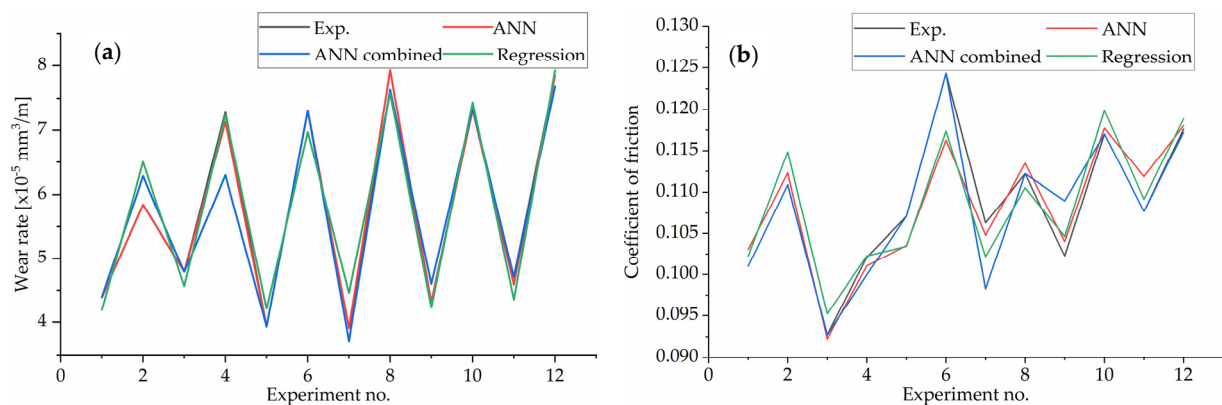
Figure 6. Comparative display of the experimental results and ANN predictions for (**a**) wear rate and (**b**) coefficient of friction.

Regression prediction results for WR and CoF, ANN prediction, and experimental results are presented in Figure 6. It can be inferred that there is a good fit between experimental and predicted results for WR, and there are some deviations from experimental results but in a small amount. For CoF, there is a higher degree of deviation between experimental and predicted results that can be attributed to the complexity of CoF's nature, which results in the regression and ANN models being less accurate.

Based on a detailed analysis of the tribological and mechanical properties of hypereutectic Al-Si alloys and composites [4], it was observed that the majority of researchers conducted tribological testing under dry conditions and with lower normal load in comparison to this investigation. Chen et al. [63] tested Al18.5Si alloy in lubricated sliding conditions with SAE 5W-30 oil, a normal load of 0.5 N, and a sliding speed of 0.05 m/s, and concluded that there was no significant wear of the tested materials. Based on these results, and the potential application of tested materials for pistons, the same lubricant was used for this investigation, but the load was selected to be 100 N and 200 N because pistons operate under high pressures. According to the [4] for Al alloys with approximately 18% Si, the average applied load was 60 N, while in the another study [58] a normal load of 100 N was applied. Analysing the results of the wear rate in the literature [11,15,57–60], it was noticed that the order of magnitude of the obtained results was in correlation with the applied testing conditions (normal load, sliding distance, and Si content in the alloy). In this paper, the addition of 3 wt.% of Al_2O_3 micro-reinforcement to the hypereutectic Al-Si base alloy resulted in an improvement in wear resistance. The same dependence was noticed by Ünlü [64], who tested an Al matrix reinforced with 3 wt.% Al_2O_3 or SiC micro-reinforcement, i.e., the composite with 3 wt.% Al_2O_3 showed better wear resistance when compared to matrix and composite containing 3 wt.% SiC. With the increase in the amount of Al_2O_3 (10–20 wt.%), further improvement in wear rate was noted [65]. In our study, the best wear resistance was noticed for composite with 0.5 wt.% Al_2O_3 nanoparticles and 3 wt.% Al_2O_3 micro-reinforcements, and the addition of SiC micro-particles improved

the wear rate when compared to the matrix alloy. Improvement in the tribological characteristics of hybrid micro/nano-reinforced Al composites was also noted by Kannan et al. [61], while Saber [64] also noticed improvement with the addition of SiC particles.

Grey analysis was performed with the application of Equations (5)–(8). Equation (9) is used when the influence of all the weights on the response is equal, but based on the delta values from Table 4, it can be inferred that there was a high influence of weight on wear rate, so the equation for the multi-response optimisation in this case is as follows:

$$\gamma_i = 0.7348 \cdot \xi_{WR}(k) + 0.2652 \cdot \xi_{CoF}(k) \tag{12}$$

where ξ_{WR} is the grey relation coefficient for WR, and ξ_{CoF} is the grey relation coefficient for CoF.

The results of the GRG obtained with Equation (10), as well as ranked values, are given in Table 3. The best combination of factors is ranked with 1, which means that the optimal wear rate and coefficient of friction are for composite with 3 wt.% Al_2O_3 microparticles (coded value 2) and 0.5 wt.% Al_2O_3 nanoparticles (coded value 2) at a normal load of 100 N (coded value 1).

Based on this research, it has been proven that developed models can be used for small data sets with high reliability, and for the optimisation and prediction of tribological characteristics.

4.3. Worn Surfaces

Microstructural characterisation of the worn surface is very complex, as well as the understanding of the wear mechanism. Figure 7 presents SEM images of worn surfaces of matrix alloy and two best-ranked combinations of factors obtained by Taguchi grey analysis (Table 3) for a normal load of 100 N. SEM analysis was carried out at the end of the tests to determine the wear mechanism of the tested materials. Figure 7, with a magnification of 500×, shows surfaces formed during sliding at 0.5 m/s sliding speed under 100 N normal load for a 1000 m sliding distance. Sliding directions are denoted with yellow-coloured arrows on Figure 7a,b. In Figure 7a, shallow grooves can be noticed which indicates mild abrasion, while there are small white fields present which indicate material transfer. For composite with 0.5 wt.% Al_2O_3 nanoparticles and 3 wt.% Al_2O_3 microparticles (Figure 7b) deeper grooves were present and bigger white fields appeared on the surface indicating transfer of the material from the steel disc to the composite block.
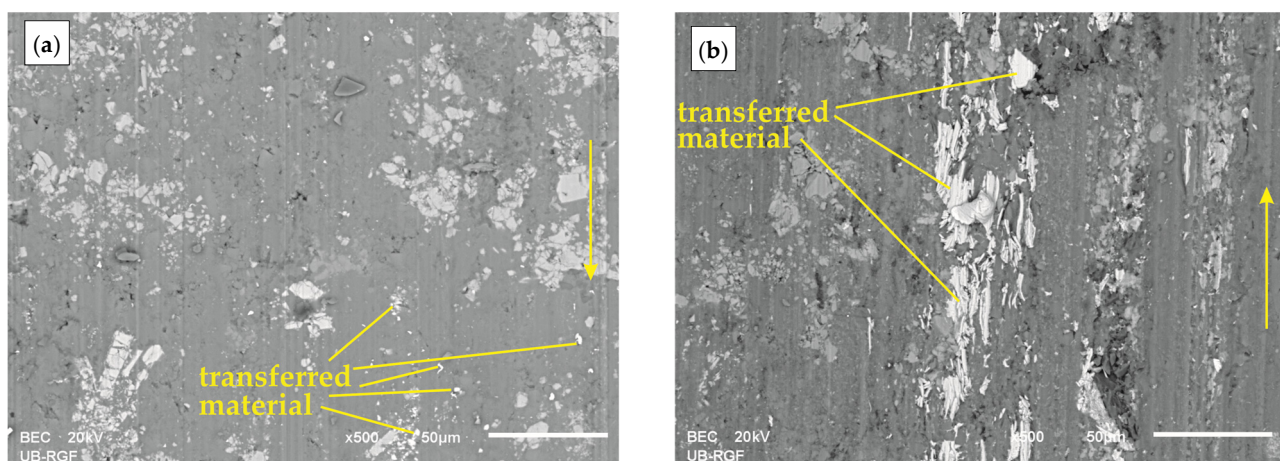
Figure 7. SEM micrograph of worn surfaces: (**a**) matrix alloy and (**b**) Al-18Si with 0.5 wt.% Al_2O_3 nanoparticles and 3 wt.% Al_2O_3 microparticles.

To confirm the material transfer, EDS analysis was performed on Al-18Si with 0.5 wt.% Al_2O_3 nanoparticles and 3 wt.% Al_2O_3 microparticles and it is presented in Figure 8.
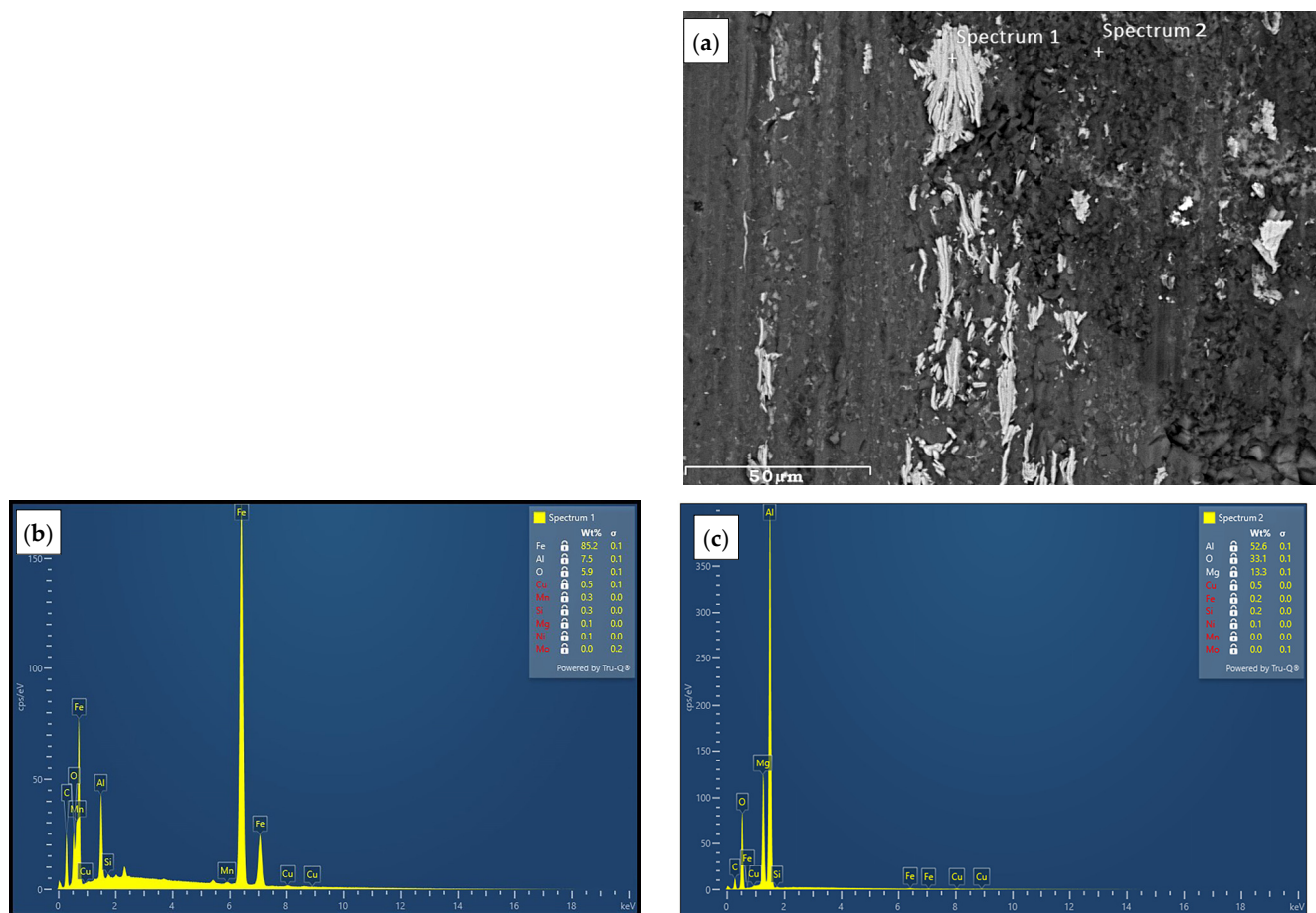
Figure 8. EDS analysis of Al-18Si with 0.5 wt.% Al_2O_3 nanoparticles and 3 wt.% Al_2O_3 microparticles tested under 100 N normal load: (**a**) spectrum positions, (**b**) Spectrum 1, and (**c**) Spectrum 2.

From Figure 8b, it can be inferred that there was Fe present on the worn surface of the composite, which indicates that the counter-body (steel disc) surface was worn and that transfer of materials from the disc occurred. The wear of the disc was mainly due to the presence of hard Al_2O_3 particles (Spectrum 2, Figure 8c).

5. Conclusions

The present research focused on the development of thixocasted/compocasted composites and hybrid composites with hypereutectic Al-18Si matrix alloy and Al_2O_3 (micro-/nano-reinforcements) or SiC micro-reinforcements by applying optimisation methods. The effects of various factors, including normal load, type of reinforcement, and amount of Al_2O_3 nano-reinforcement on the wear rate and coefficient of friction were analysed.

To obtain the best prediction of wear rate and coefficient of friction with ANNs, diverse ANNs were used. The optimal ANN model for wear rate, a backpropagation network with 3-15-1 architecture, and a logsig transfer function, displayed exceptional accuracy with an overall regression coefficient of 0.99484. This network showed a good correlation between experimental and predicted results, even with the small data set. For the prediction of the coefficient of friction, the backpropagation network with a 3-6-1 architecture and tansig transfer function exhibited an overall regression coefficient of 0.93096. When the ANN was used to predict the behaviour of both the wear rate and coefficient of friction, it did not give a good prediction. Due to deviations in the coefficient of friction for two outputs in this case, it is better to use ANNs for wear rate and coefficient of friction separately.

After ANN selection, Taguchi analysis for single response optimisation was performed to obtain the optimal combination of factors that impact wear rate and coefficient of

friction. Minimal wear rate, according to Taguchi analysis, was obtained for the following combination of factors A2-B1-C1 (composite with 3 wt.% Al_2O_3 micro-reinforcement and without Al_2O_3 nano-reinforcement at a normal load of 100 N). The optimal combination of factors for the friction coefficient was A1-B2-C1 (composite with 0.5 wt.% Al_2O_3 nano-reinforcement at a normal load of 100 N). From the ANOVA, it was determined that the most influential factor on wear rate was the normal load at 92.33%, while the most influential factors on coefficient of friction were the normal load and type of micro-reinforcement at 45.18 and 35.00%, respectively. For wear rate, the influence of interactions between factors was highest for the type of micro-reinforcement and normal load (A × C), while for the coefficient of friction, the highest interaction of factors was for the type of micro-reinforcement and amount of Al_2O_3 nanoparticles (A × B).

The development of the regression model gave very good prediction results, i.e., both ANNs for one output and regression showed a very good correlation to the experimental results. An optimal combination for wear rate and coefficient of friction was determined with a Taguchi grey multi-response optimisation methodology. The optimal combination of factors was obtained for a composite with a 3 wt.% Al_2O_3 micro-reinforcement and 0.5 wt.% Al_2O_3 nanoparticles at a normal load of 100 N. Wear rate had a higher influence on grey analysis than CoF, and thus on optimal combination of factors. The optimal combination of factors caused the wear rate lower than the matrix alloy by 11%.

This research showed that the application of optimisation methods can be used for small data sets. The results of this research can contribute to future research on hypereutectic Al-Si composites and the potential practical application of hybrid composites for the production of pistons.

Author Contributions: Conceptualisation, S.M. and A.V.; methodology, B.S. and A.V.; experimental design, S.G.; experiments, S.M.; optimisation, S.G.; formal analysis, S.M.; validation, S.S. and I.M.; draft writing, S.M.; review and editing, S.S. and A.V.; proofreading, I.M. and A.V.; supervision, B.S. and A.V.; funding acquisition, A.V. All authors have read and agreed to the published version of the manuscript.

References

1. Joseph, R. Davis Aluminum and Aluminum Alloys. In *Alloying: Understanding the Basics*; ASM International: Almere, The Netherlands, 2001; pp. 351–416, ISBN 978-0-87170-744-4.
2. Jorstad, J.; Apelian, D. Hypereutectic Al-Si Alloys: Practical Casting Considerations. *Int. J. Met.* **2009**, *3*, 13–36. [CrossRef]
3. Wang, K.; Wei, M.; Zhang, L.; Du, Y. Morphologies of Primary Silicon in Hypereutectic Al-Si Alloys: Phase-Field Simulation Supported by Key Experiments. *Metall. Mater. Trans. A* **2016**, *47*, 1510–1516. [CrossRef]
4. Miladinović, S.; Stojanović, B.; Gajević, S.; Vencl, A. Hypereutectic Aluminum Alloys and Composites: A Review. *Silicon* **2023**, *15*, 2507–2527. [CrossRef]
5. Bleck, W.; Dziallach, S.; Meuser, H.; Püttgen, W.; Uggowitzer, P.J. Material Aspects of Steel Thixoforming. In *Thixoforming: Semi-solid Metal Processing*; Wiley: Hoboken, NJ, USA, 2009; pp. 43–104, ISBN 978-3-527-62396-9.
6. Husain, N.; Ahmad, A. An Overview of Thixoforming Process. *IOP Conf. Ser. Mater. Sci. Eng.* **2017**, *257*, 12053. [CrossRef]
7. Birol, Y. Cooling Slope Casting and Thixoforming of Hypereutectic A390 Alloy. *J. Mater. Process. Technol.* **2008**, *207*, 200–203. [CrossRef]
8. Hekmat-Ardakan, A.; Liu, X.; Ajersch, F.; Chen, X.-G. Wear Behaviour of Hypereutectic Al–Si–Cu–Mg Casting Alloys with Variable Mg Contents. *Wear* **2010**, *269*, 684–692. [CrossRef]
9. Lasa, L.; Rodriguez-Ibabe, J.M. Effect of Composition and Processing Route on the Wear Behaviour of Al–Si Alloys. *Scr. Mater.* **2002**, *46*, 477–481. [CrossRef]

10. Lasa, L.; Rodriguez-Ibabe, J.M. Wear Behaviour of Eutectic and Hypereutectic Al–Si–Cu–Mg Casting Alloys Tested against a Composite Brake Pad. *Mater. Sci. Eng. A* **2003**, *363*, 193–202. [CrossRef]

11. Singhal, V.; Gupta, A.; Pandey, O.P. Dry Sliding Wear Behavior of Tempered (T4 and T6) Hypereutectic Aluminum Alloy-Based Composites. *Silicon* **2023**, *15*, 897–912. [CrossRef]

12. Reddy, T.V.S.; Dwivedi, D.K.; Jain, N.K. Adhesive Wear of Stir Cast Hypereutectic Al–Si–Mg Alloy under Reciprocating Sliding Conditions. *Wear* **2009**, *266*, 1–5. [CrossRef]

13. Wang, F.; Ma, Y.; Zhang, Z.; Cui, X.; Jin, Y. A Comparison of the Sliding Wear Behavior of a Hypereutectic Al–Si Alloy Prepared by Spray-Deposition and Conventional Casting Methods. *Wear* **2004**, *256*, 342–345. [CrossRef]

14. Khemraj, S.; Jha, A.K.; Ojha, S.N. Tribo-Mechanical Behavior of Complex Hypereutectic Al–Si Alloy Compressed through a Converging Die at Elevated Temperatures. *Mater. Res. Express* **2018**, *5*, 76509. [CrossRef]

15. Li, R.; Liu, L.; Zhang, L.; Sun, J.; Shi, Y.; Yu, B. Effect of Squeeze Casting on Microstructure and Mechanical Properties of Hypereutectic Al-xSi Alloys. *J. Mater. Sci. Technol.* **2017**, *33*, 404–410. [CrossRef]

16. Han, Q.; Setchi, R.; Evans, S.L. Synthesis and Characterisation of Advanced Ball-Milled Al-Al$_2$O$_3$ Nanocomposites for Selective Laser Melting. *Powder Technol.* **2016**, *297*, 183–192. [CrossRef]

17. Mazahery, A.; Abdizadeh, H.; Baharvandi, H.R. Development of High-Performance A356/Nano-Al$_2$O$_3$ Composites. *Mater. Sci. Eng. A* **2009**, *518*, 61–64. [CrossRef]

18. Gajević, S.; Miladinović, S.; Ivanovic, L.; Skulić, A.; Stojanović, B. A Review on Mechanical Properties of Aluminium-Based Metal Matrix Nanocomposites. *Tribol. Mater.* **2023**, *2*, 114–127. [CrossRef]

19. Durai, T.G.; Das, K.; Das, S. Synthesis and Characterization of Al Matrix Composites Reinforced by in Situ Alumina Particulates. *Mater. Sci. Eng. A* **2007**, *445–446*, 100–105. [CrossRef]

20. Stojanović, B.; Gajević, S.; Kostić, N.; Miladinović, S.; Vencl, A. Optimization of Parameters That Affect Wear of A356/AlO Nanocomposites Using RSM, ANN, GA and PSO Methods. *Ind. Lubr. Tribol.* **2022**, *74*, 350–359. [CrossRef]

21. Sajjadi, S.A.; Ezatpour, H.R.; Beygi, H. Microstructure and Mechanical Properties of Al–Al$_2$O$_3$ Micro and Nano Composites Fabricated by Stir Casting. *Mater. Sci. Eng. A* **2011**, *528*, 8765–8771. [CrossRef]

22. Nirala, A.; Soren, S.; Kumar, N.; Dwivedi, V.K.; Kaushal, D.R. A Comprehensive Review on Stir Cast Al-SiC Composite. *Int. Conf. Mech. Energy Technol.* **2020**, *21*, 1610–1614. [CrossRef]

23. Rana, R.S.; Purohit, R.; Soni, V.K.; Das, S. Characterization of Mechanical Properties and Microstructure of Aluminium Alloy-SiC Composites. *Mater. Today Proc.* **2015**, *2*, 1149–1156. [CrossRef]

24. Nagaraj, A.; Gopalakrishnan, S. A Study on Mechanical and Tribological Properties of Aluminium 1100 Alloys 6% of RHAp, BAp, CSAp, ZnOp and Egg Shellp Composites by ANN. *Silicon* **2021**, *13*, 3367–3376. [CrossRef]

25. Karabulut, Ş.; Karakoç, H. Investigation of Surface Roughness in the Milling of Al7075 and Open-Cell SiC Foam Composite and Optimization of Machining Parameters. *Neural Comput. Appl.* **2017**, *28*, 313–327. [CrossRef]

26. Ekka, K.K.; Chauhan, S.R. Varun Dry Sliding Wear Characteristics of SiC and Al$_2$O$_3$ Nanoparticulate Aluminium Matrix Composite Using Taguchi Technique. *Arab. J. Sci. Eng.* **2015**, *40*, 571–581. [CrossRef]

27. Ajith Arul Daniel, S.; Pugazhenthi, R.; Kumar, R.; Vijayananth, S. Multi Objective Prediction and Optimization of Control Parameters in the Milling of Aluminium Hybrid Metal Matrix Composites Using ANN and Taguchi-Grey Relational Analysis. *Def. Technol.* **2019**, *15*, 545–556. [CrossRef]

28. Hussain, M.Z.; Khan, S.; Sarmah, P. Optimization of Powder Metallurgy Processing Parameters of Al$_2$O$_3$/Cu Composite through Taguchi Method with Grey Relational Analysis. *J. King Saud Univ.—Eng. Sci.* **2020**, *32*, 274–286. [CrossRef]

29. Dey, D.; Bhowmik, A.; Biswas, A. Tribological Performance Optimization of Al2024-TiB2 Composites Using Grey-Taguchi Approach. *Int. J. Cast Met. Res.* **2022**, *35*, 144–151. [CrossRef]

30. Khatkar, S.K.; Suri, N.M.; Kant, S.; Pankaj. A Review on Mechanical and Tribological Properties of Graphite Reinforced Self Lubricating Hybrid Metal Matrix Composites. *Rev. Adv. Mater. Sci.* **2018**, *56*, 1–20. [CrossRef]

31. Kandpal, B.C.; kumar, J.; Singh, H. Fabrication and Characterisation of Al$_2$O$_3$/Aluminium Alloy 6061 Composites Fabricated by Stir Casting. *Mater. Today Proc.* **2017**, *4*, 2783–2792. [CrossRef]

32. Ashwath, P.; Xavior, M.A. Processing Methods and Property Evaluation of Al$_2$O$_3$ and SiC Reinforced Metal Matrix Composites Based on Aluminium 2xxx Alloys. *J. Mater. Res.* **2016**, *31*, 1201–1219. [CrossRef]

33. Sajjadi, S.A.; Ezatpour, H.R.; Torabi Parizi, M. Comparison of Microstructure and Mechanical Properties of A356 Aluminum Alloy/Al$_2$O$_3$ Composites Fabricated by Stir and Compo-Casting Processes. *Mater. Des.* **2012**, *34*, 106–111. [CrossRef]

34. Veličković, S.; Stojanović, B.; Babić, M.; Vencl, A.; Bobić, I.; Vadászné Bognár, G.; Vučetić, F. Parametric Optimization of the Aluminium Nanocomposites Wear Rate. *J. Braz. Soc. Mech. Sci. Eng.* **2018**, *41*, 19. [CrossRef]

35. Dochev, B.; Panov, I.; Dimova, D. Study of the Retention of the Modifying Effect of a Nanodiamond Nanomodifier on the Structure of AlSi18 Alloy. *AIP Conf. Proc.* **2024**, *2980*, 60013. [CrossRef]

36. Hekmat-Ardakan, A.; Ajersch, F. Effect of Conventional and Rheocasting Processes on Microstructural Characteristics of Hypereutectic Al–Si–Cu–Mg Alloy with Variable Mg Content. *J. Mater. Process. Technol.* **2010**, *210*, 767–775. [CrossRef]

37. Choi, H.; Konishi, H.; Li, X. Al$_2$O$_3$ Nanoparticles Induced Simultaneous Refinement and Modification of Primary and Eutectic Si Particles in Hypereutectic Al–20Si Alloy. *Mater. Sci. Eng. A* **2012**, *541*, 159–165. [CrossRef]

38. Choi, H.; Li, X. Preparationand Characterization of Hypereutectic Al-20wt.%Si-4.5wt.%Cu Nanocomposites with Al$_2$O$_3$ Nnanoparticles. In *Research and Markets, Proceedings of the TMS 2011 140th Annual Meeting and Exhibition Supplemental Proceedings: General Paper Selections, San Diego, CA, USA, 27 March 2011*; John Wiley & Sons, Inc.: Hoboken, NJ, USA, 2011; Volume 3, pp. 117–122.

39. El Mahallawi, I.; Shash, Y.; Rashad, R.M.; Abdelaziz, M.H.; Mayer, J.; Schwedt, A. Hardness and Wear Behaviour of Semi-Solid Cast A390 Alloy Reinforced with Al$_2$O$_3$ and TiO$_2$ Nanoparticles. *Arab. J. Sci. Eng.* **2014**, *39*, 5171–5184. [CrossRef]

40. El-Mahallawi, I.S.; Shash, A.Y. Mechanical Properties and Wear Resistance of Semisolid Cast Al$_2$O$_3$ Nano Reinforced Hypo and Hyper-Eutectic Al–Si Composites. In *Properties and Characterization of Modern Materials*; Öchsner, A., Altenbach, H., Eds.; Springer: Singapore, 2017; pp. 13–30, ISBN 978-981-10-1602-8.

41. Santos, J.; Jarfors, A.E.W.; Dahle, A.K. Formation of Iron-Rich Intermetallic Phases in Al-7Si-Mg: Influence of Cooling Rate and Strontium Modification. *Metall. Mater. Trans. A* **2019**, *50*, 4148–4165. [CrossRef]

42. Yu, J. Formation of Intermetallic Phases in Al-10Si-0.3Fe Based Alloys. Ph.D. Thesis, Technischen Universität Berlin, Berlin, Germany, 2016.

43. Rios, C.; Caram, R.; Botta, W.F.; Kiminam, C.; Bolfarini, C. Intermetallic Compounds in the Al-Si-Cu System. *Acta Microsc.* **2003**, *12*, 77–82.

44. Warmuzek, M. Chemical Composition of the Ni-Containing Intermetallic Phases in the Multicomponent Al Alloys. *J. Alloys Compd.* **2014**, *604*, 245–252. [CrossRef]

45. Milojević, S.; Savić, S.; Maric, D.; Stopka, O.; Krstić, B.; Stojanovic, B. Correlation between Emission and Combustion Characteristics with the Compression Ratio and Fuel Injection Timing in Tribologically Optimized Diesel Engine. *Teh. Vjesn.* **2022**, *29*, 1210–1219. [CrossRef]

46. Kaminaga, T.; Yamaguchi, K.; Ratnak, S.; Kusaka, J.; Youso, T.; Fujikawa, T.; Yamakawa, M. *A Study on Combustion Characteristics of a High Compression Ratio SI Engine with High Pressure Gasoline Injection*; SAE International: Warrendale, PA, USA, 2019.

47. Mishra, S.K.; Brahma, A.; Dutta, K. Prediction of Mechanical Properties of Al-Si-Mg Alloy Using Artificial Neural Network. *Sādhanā* **2021**, *46*, 139. [CrossRef]

48. Khishe, M.; Parvizi, G.R. Artificial Neural Networks, Concept, Application and Types. In *Neural Networks*; Nova Science Publishers, Inc.: Hauppauge, NY, USA, 2020; pp. 1–30, ISBN 978-1-5361-7188-4.

49. Tosh, C.R.; Ruxton, G.D. (Eds.) *Modelling Perception with Artificial Neural Networks*; Cambridge University Press: Cambridge, UK, 2010; ISBN 978-0-521-76395-0.

50. Zohuri, B.; Moghaddam, M. *Neural Network Driven Artificial Intelligence: Decision Making Based on Fuzzy Logic*; Nova Science Publishers, Inc.: Hauppauge, NY, USA, 2017; ISBN 978-1-5361-2114-8.

51. Kumar, P.; Gururaj, S. Conceptual Cost Modelling for Sustainable Construction Project Planning—A Levenberg–Marquardt Neural Network Approach. *Appl. Math. Inf. Sci.* **2019**, *13*, 201–208. [CrossRef]

52. Ranganathan, S.; Manivannan, I. Evaluation of Tribological Process Parameters of Al6061 + Nano Sic + Gr Hybrid Nano Composites Using Taguchi Technique. *Mater. Today Proc.* **2023**, *in press*. [CrossRef]

53. Kelsy, B.; Nwobi-Okoye, C.; Chukwuemeka, E.; Uche, R. Multi Objective Optimization of Novel Al-Si-Mg Nanocomposites: A Taguchi-ANN-NSGA-II Approach. *J. Eng. Res.* **2023**, *in press*. [CrossRef]

54. Dhiman, M.; Dwivedi, D.K.; Sehgal, R.; Bhat, I. Effect of Iron on Wear Behavior of As-Cast and Heat-Treated Hypereutectic Al–18Si–4Cu–0.5Mg Alloy: A Taguchi Approach. *Proc. Inst. Mech. Eng. Part J. Mater. Des. Appl.* **2014**, *228*, 2–16. [CrossRef]

55. Marode, R.V.; Pedapati, S.R.; Lemma, T.A.; Loyte, A.; Devarajan, Y.; Thandavamoorthy, R. Influence of Silicon Carbide on Microhardness and Corrosion Behavior of AZ91/SiC Surface Composites Processed through Friction Stir Processing: Multi-Response Optimization Using Taguchi-Grey Relational Analysis. *Silicon* **2023**, *15*, 6921–6943. [CrossRef]

56. Kumar, S.; Priyadarshan; Ghosh, S.K. Statistical and Artificial Neural Network Technique for Prediction of Performance in AlSi10Mg-MWCNT Based Composite Materials. *Mater. Chem. Phys.* **2021**, *273*, 125136. [CrossRef]

57. Singhal, V.; Pandey, O.P. Wear and Friction Behavior of Gr/Sn Solid Lubricated Dual Reinforced AMCs. *Silicon* **2022**, *14*, 5629–5645. [CrossRef]

58. Abouei, V.; Shabestari, S.G.; Saghafian, H. Dry Sliding Wear Behaviour of Hypereutectic Al–Si Piston Alloys Containing Iron-Rich Intermetallics. *Mater. Charact.* **2010**, *61*, 1089–1096. [CrossRef]

59. Jena, K.P.; Majhi, J.; Sahoo, S.K.; Pattnaik, S.C. The Microstructural and Wear Properties Improvement by Manganese Addition in Al-14Si Hypereutectic Alloy. *Mater. Today Proc.* **2022**, *62*, 5934–5941. [CrossRef]

60. Jayakumar, E.; Varghese, T.; Rajan, T.P.D.; Pai, B.C. Reciprocating Wear Analysis of Magnesium-Modified Hyper-Eutectic Functionally Graded Aluminium Composites. *Trans. Indian Inst. Met.* **2019**, *72*, 1643–1649. [CrossRef]

61. Kannan, P.R.; Thanigaivelan, R.; Thiraviam, R.; Pradeep Kumar, K. Performance Studies on Hybrid Nano-Metal Matrix Composites for Wear and Surface Quality. *Mater. Sci.-Pol.* **2023**, *41*, 288–300. [CrossRef]

62. Turan, M.; Aydın, F.; Sun, Y.; Zengin, H.; Akinay, Y. Wear Resistance and Tribological Properties of GNPs and MWCNT Reinforced AlSi18CuNiMg Alloys Produced by Stir Casting. *Tribol. Int.* **2021**, *164*, 107201. [CrossRef]

63. Chen, M.; Alpas, A.T. Ultra-Mild Wear of a Hypereutectic Al–18.5wt.% Si Alloy. *Wear* **2008**, *265*, 186–195. [CrossRef]

64. Ünlü, B.S. Investigation of Tribological and Mechanical Properties Al$_2$O$_3$–SiC Reinforced Al Composites Manufactured by Casting or P/M Method. *Mater. Des.* **2008**, *29*, 2002–2008. [CrossRef]
65. Saber, D. Improvement of tribological properties of A356-Al$_2$O$_3$ cast composites by heat-treatment. *J. Al-Azhar Univ. Eng. Sect.* **2018**, *13*, 998–1003. [CrossRef]